Supporting Information for

Large spatial heterogeneity in historical atmospheric sulfate trends over the Tibetan Plateau inferred from ice-core records

Hongcheng Lu[1], Peng Wang[1], Dandan Yang[2], Tandong Yao[2], Guangjian Wu[2], Huabiao Zhao[2], Xiangying Li[3], and Lei Geng[1, 4, 5]

Correspondence: Lei Geng (genglei@ustc.edu.cn)

[1]National Key Laboratory of Deep Space Exploration/School of Earth and Space Sciences, University of Science and Technology of China, Hefei, China

[2]State Key Laboratory of Tibetan Plateau Earth System, Environment and Resources (TPESER), Institute of Tibetan Plateau Research, Chinese Academy of Sciences, Beijing, China

[3]Shaanxi Key Laboratory of Earth Surface System and Environmental Carrying Capacity, Northwest University, Xi'an, China

[4]Deep Space Exploration Laboratory, Hefei, China

[5]CAS Center for Excellence in Comparative Planetology, University of Science and Technology of China, Hefei, China

Contents

• Text S1. Precipitation comparison

• Table S1. Agreement with CRU TS4.07 and ERA5 across six regions (1940–2014).

• Table S2. CMIP6 historical simulations used in this study, including model identifiers, variables, ensemble members, grid labels, data versions, and their use in the analyses.

• Figure S1. Temporal coverage of the ice core records across the Tibetan Plateau.

• Figure S2. Comparison of dry sulfate (SO_4^{2-}) deposition results simulated by different models at six regions across the Tibetan Plateau.

• Figure S3.Comparison of wet sulfate (SO_4^{2-}) deposition results simulated by different models at six regions across the Tibetan Plateau.

• Figure S4.Modeled precipitation time series for different ice core sites across the Tibetan Plateau using various climate models.

Text S1 Precipitation comparison

Precipitation from the 11 CMIP6 models was compared with Climatic Research Unit Time-Series version 4.07 (CRU TS4.07; Harris et al., 2020) and the European Centre for Medium-Range Weather Forecasts fifth-generation reanalysis (ERA5; Hersbach et al., 2020) for 1940–2014. Annual precipitation was averaged with equal weight across the sites in each region. We evaluated three complementary properties: the median absolute percentage difference in regional mean precipitation, the mean Spearman correlation of the regional wet-to-dry ordering, and the median absolute difference in percentage change between 1940–1969 and 1985–2014. The six regions and the two reference products received equal weight. These metrics diagnose different aspects of performance (Table S1).

CESM2-WACCM was retained for the named sensitivity analysis because it combines vertically resolved interactive chemistry and detailed aerosol treatment with comparatively strong precipitation-pattern and change metrics. Its regional wet-to-dry ordering correlation is $\rho = 0.80$, tied for the highest value, and its early-to-late change difference is 4.98 percentage points, the fourth-smallest value. Its magnitude-difference metric is 105.3 % (rank 9 of 11). The sign of the ice-core flux-proxy change was also evaluated with precipitation from all 11 models, their multi-model median, CRU TS4.07, and ERA5. Across these 14 products, the sign is stable in NW1, MD1, MD3, and SO1 but varies in NE1 and MD2.

Table S1. Agreement of CMIP6 precipitation with CRU TS4.07 and ERA5 across six regions for 1940–2014. Values are metric values followed by ranks in parentheses (1 = best); pp denotes percentage points.

Model	Magnitude difference (%)	Spatial agreement (ρ)	Change difference (pp)
IPSL-CM5A2-INCA	59.9 (2)	0.29 (9)	6.95 (7)
IPSL-CM6A-LR-INCA	85.8 (6)	0.14 (11)	3.70 (1)
MIROC-ES2L	96.0 (7)	0.57 (5)	4.08 (2)
MIROC6	128.0 (11)	0.46 (8)	5.12 (5)
UKESM1-0-LL	64.1 (3)	0.29 (9)	10.92 (10)
MPI-ESM-1-2-HAM	46.0 (1)	0.63 (4)	4.90 (3)
MRI-ESM2-0	82.4 (5)	0.49 (7)	5.72 (6)
GISS-E2-1-H	78.9 (4)	0.57 (5)	11.52 (11)
CESM2	107.7 (10)	0.80 (1)	7.91 (9)
CESM2-FV2	102.0 (8)	0.71 (3)	7.47 (8)
CESM2-WACCM	105.3 (9)	0.80 (1)	4.98 (4)

Table S2. CMIP6 historical simulations used in this study, including model identifiers, variables, ensemble members, grid labels, data versions, and their use in the analyses.

Model	mmrso4 member	dryso4 / wetso4 member	Grid label
IPSL-CM5A2-INCA	r1i1p1f1	r1i1p1f1	gr
IPSL-CM6A-LR-INCA	r1i1p1f1	r1i1p1f1	gr
MIROC-ES2L	r1i1p1f2	r1i1p1f2	gn
MIROC6	r1i1p1f1	r1i1p1f1	gn
UKESM1-0-LL	r13i1p1f2	r13i1p1f2	gn
MPI-ESM-1-2-HAM	r3i1p1f1	r3i1p1f1	gn
MRI-ESM2-0	r7i1p1f1	r7i1p1f1	gn
GISS-E2-1-H	r1i1p3f1	r1i1p3f1	gn
CESM2	r1i1p1f1	r1i1p1f1	gn
CESM2-FV2	r1i1p1f1	r1i1p1f1	gn
CESM2-WACCM	r1i1p1f1	r1i1p1f1	gn

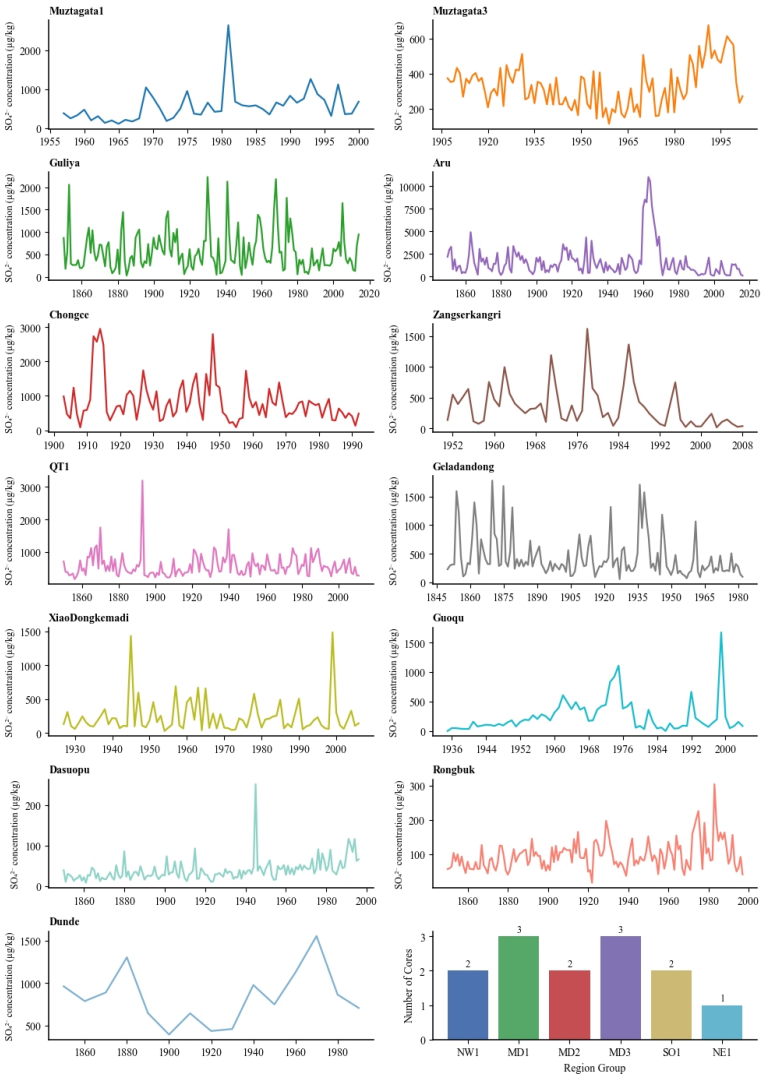


Figure S1. Temporal coverage of the ice core records across the Tibetan Plateau.

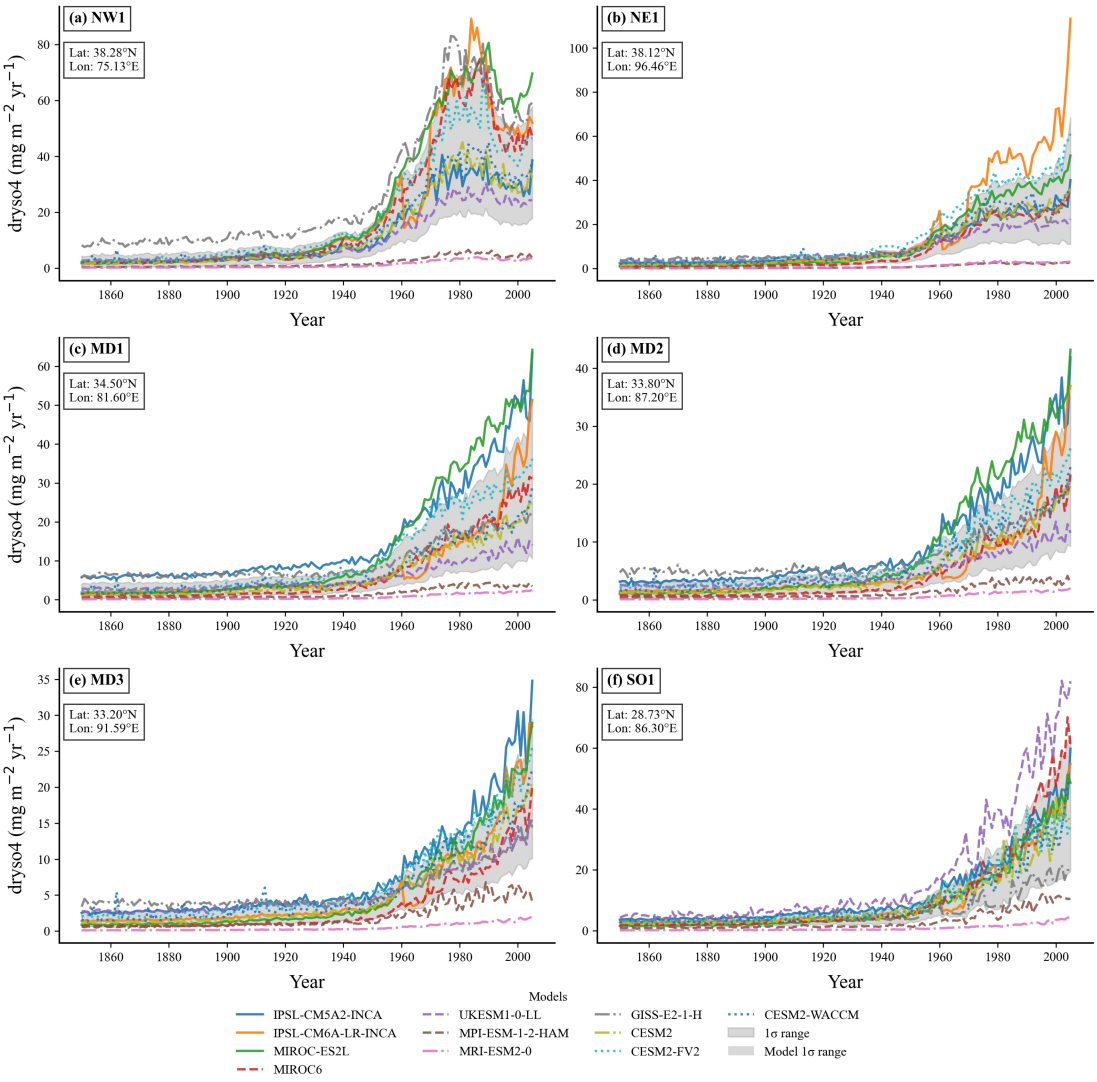


Figure S2. Comparison of dry sulfate (SO_4^{2-}) deposition results simulated by different models for (a) NW1, (b) NE1, (c) MD1, (d) MD2, (e) MD3, and (f) SO1 across the Tibetan Plateau.

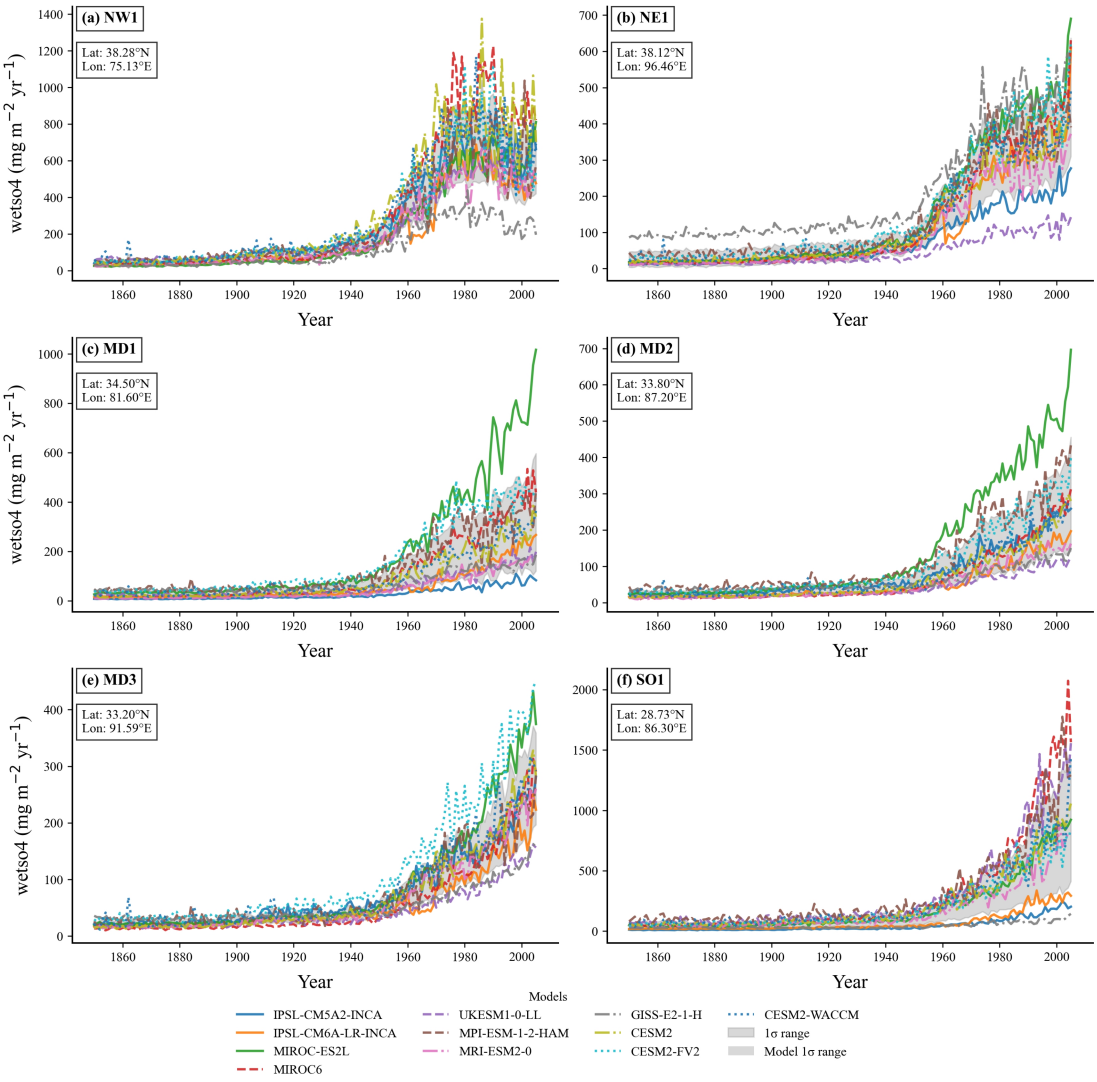


Figure S3. Comparison of wet sulfate (SO_4^{2-}) deposition results simulated by different models for (a) NW1, (b) NE1, (c) MD1, (d) MD2, (e) MD3, and (f) SO1 across the Tibetan Plateau.

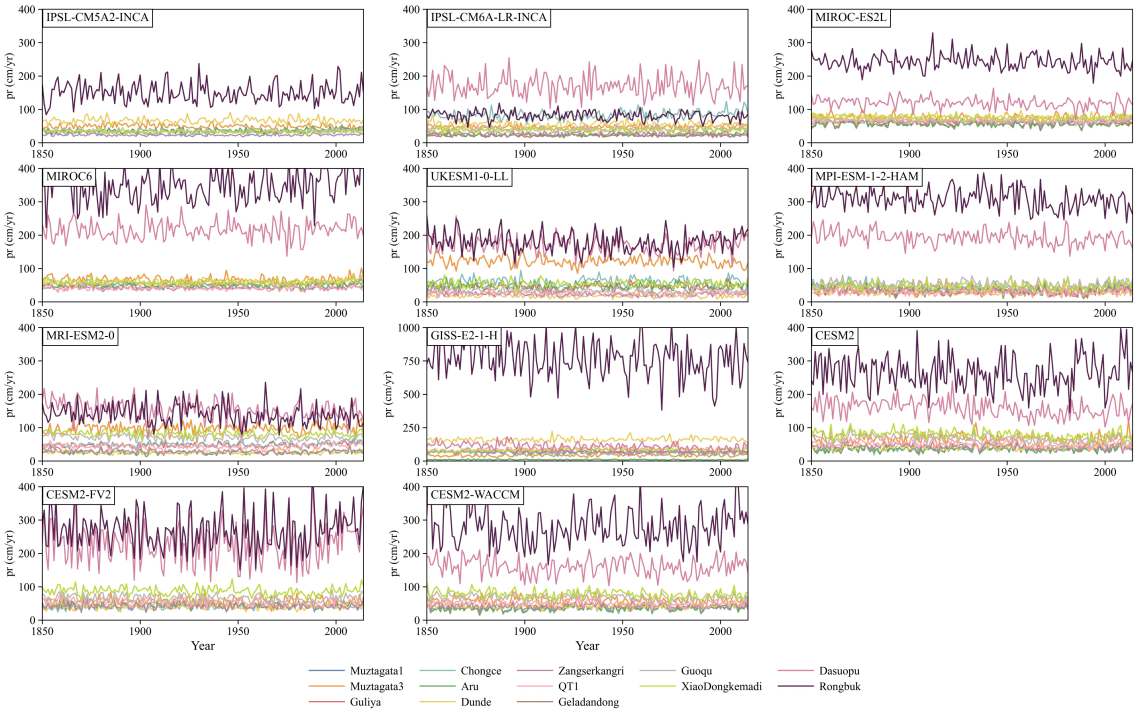


Figure S4. Modeled precipitation time series for different ice core sites across the Tibetan Plateau using various climate models.

References

Harris, I., T. J. Osborn, P. Jones, and D. Lister, 2020: Version 4 of the CRU TS monthly high-resolution gridded multivariate climate dataset. Scientific Data, 7, 109, https://doi.org/10.1038/s41597-020-0453-3.

Hersbach, H., and Coauthors, 2020: The ERA5 global reanalysis. Quarterly Journal of the Royal Meteorological Society, 146, 1999–2049, https://doi.org/10.1002/qj.3803.